Bulletin of the Mineral Research and Exploration

http://bulletin.mta.gov.tr

Magmatic significance and hydrothermal alteration of layered chromitites from the Bracco Gabbro Complex, Ligurian Ophiolites, Italy

Federica ZACCARINI[*a], Raphael J. BAUMGARTNER[b], Constantinos MAVROGONATOS[c] and Giorgio GARUTI[a]

[a]*Geosciences Programme, Faculty of Science, University Brunei Darussalam, Jalan Tungku Link, Bandar Seri Begawan BE1410, Brunei*
[b]*CSIRO Mineral Resources, Australian Resources Research Centre, Kensington, WA 6151, Australia*
[c]*Dipartimento di Scienze della Terra, Università di Pisa, Via Santa Maria 53, I-56126 Pisa, Italy*

Research Article

Keywords:
Ophiolite, Bracco Gabbro Complex, Chromitites, Hydrothermal Alteration, Chlorite Thermometry, Apennines, Northern Italy.

ABSTRACT

The Bracco chromitites are hosted in the Mesozoic Ligurian Ophiolites (Italy) and provide key insights into the magmatic and post-magmatic (i.e. metamorphic and hydrothermal) evolution of gabbro-hosted chromitites in an oceanic mantle. Petrographic and mineralogical analyses reveal that the Bracco chromitites comprise cumulitic, massive to disseminated, layered chromitites overprinted by multi-stage alteration within altered olivine–clinopyroxene–anorthite cumulates. Detailed Cr–Al–Fe^{3+} systematics indicates that primary Cr- to Al-rich chromite, affected by metamorphic-hydrothermal processes under sub-greenschist facies conditions, locally escaped recrystallization and metasomatic modification. Consequently, chromite cores preserve their primary magmatic compositions consistent with crystallization from aluminous melts produced by low-degree partial mantle melting at a mid-ocean ridge (MOR) setting. Metamorphic-hydrothermal alteration is marked by multi-stage ferrian chromite rims, whereas based on their Mg content the associated chlorite is classified as clinochlore. Chlorite geothermometry indicates alteration temperatures in the range of ~100-300 °C, consistent with oceanic serpentinization under prehnite-pumpellyite facies conditions. The hydrothermal fluids were oxidizing, enriched in SiO_2 and MnO, and circulated through fracture networks in the shallow oceanic lithosphere. Elevated MnO amounts in alteration rims suggest widespread Mn-enrichment in these fluids, potentially linking them to seafloor Mn deposits in the Ligurian Ophiolites. Together, these findings indicate that the Bracco chromitites, their gabbroic hosts, and associated lherzolitic mantle rocks were at least partially exposed at the Tethyan seafloor prior to their final emplacement during the Alpine orogenetic phase, where serpentinization promoted complex chromite alteration.

Received Date: 13.05.2025
Accepted Date: 06.08.2025

1. Introduction

Massive chromitites are predominantly composed of chromite, a spinel-group mineral with a broad solid- solution range in which Cr, along with Al and Fe^{3+}, are the principal trivalent cations; Mg and Fe^{2+} are the dominant bivalent ones (Stowe, 1994; Bosi et al., 2019). Chromite is the sole economic source of Cr, mined from both stratiform chromitites hosted in mafic-ultramafic layered complexes within cratonic regions and podiform chromitites in the oceanic mantle (Thayer, 1970).

Citation Info: Zaccatini, F., Baumgartner, R. J., Mavrogonatos, C., Garuti, G. 2025. Magmatic significance and hydrothermal alteration of layered chromitites from the Bracco Gabbro Complex Ophiolite, Ligurian Ophiolites, Italy. Bulletin of the Mineral Research and Exploration 178, 113-129. https://doi.org/10.19111/bulletinofmre.1764813

**Corresponding author: Federica ZACCARINI, federicazaccarinigaruti@gmail.com*

A chromian spinel is among the first refractory minerals to crystallize from mafic to ultramafic magmas at temperatures above 1000 °C. Owing to its high resistance to post-magmatic alteration, especially relative to olivine and pyroxene, chromite composition is a valuable petrogenetic indicator for constraining parameters like the parental magma composition, tectonic setting, and the degree of partial melting of the mantle (Irvine, 1965; Dick and Bullen, 1984; Stowe, 1994; Zhou and Robinson, 1994; Zhou et al., 1998; Barnes and Roeder, 2001; Kamenetsky et al., 2002; Arai et al., 2004). For example, the ratio Cr/Al in magmatic chromite, expressed as Cr# [Cr/(Cr + Al)], classifies ophiolitic chromitites as Cr-rich (Cr# > 0.7) or Al-rich (Cr# < 0.6; Zhou et al., 1998). The distribution of high-Cr versus high-Al chromitites reflects the geotectonic setting (e.g., subduction-related versus non-subduction), and the nature of the ultramafic mantle, whether depleted or fertile, depending on prior melt extraction (Leblanc and Nicolas, 1992; Boudier and Al-Rajhi, 2014).

Integrating Mg# [Mg/(Mg + Fe)] and Cr_2O_3–TiO_2 systematics further refines chromitite classification (podiform vs. stratiform) and aids in linking chromitite formation to broader tectonic settings and mantle melting regimes, such as island-arc versus mid-ocean ridge (MOR) environments (e.g., Kamenetsky et al., 2002; Arai et al., 2004).

The primary magmatic composition of chromite in both podiform and stratiform chromitites can be partially or entirely overprinted by metamorphic and hydrothermal alteration, leading to the formation a rim of secondary oxide (Irvine, 1965; Evans and Frost, 1975; Loferski, 1986; Burkhard, 1993; De Freitas Suita and Strieder, 1996; Barnes, 2000; Barnes and Roeder, 2001; Mellini et al., 2005; Gervilla et al., 2012). Simple models for chromite alteration in ophiolitic mantle rocks link the formation of ferrian chromite from magmatic chromite to low-temperature serpentinization (≤400 °C), involving progressive leaching of Mg and relative enrichment in Fe^{3+} over Al and Cr under hydrous, oxidizing conditions (Loferski, 1986; Burkhard, 1993). Specifically, ferrian chromite may form during retrograde metamorphism under similar hydrous, oxidizing conditions, possibly even involving multi-stage reactions between chromite and progressively altered host-rock mineralogy across varying temperatures and redox states (Garuti et al., 2007; 2012; Gervilla et al., 2012).

Some investigators have suggested, however, that chromite alteration may take place during prograde metamorphism leading to the formation of chromian magnetite under greenschist-facies conditions and subsequent transformation to ferrian chromite at amphibolite-facies metamorphism (Bliss and MacLean, 1975; Barnes, 2000; Merlini et al., 2009; Gervilla et al., 2012). Regardless of the specific tectono-metamorphic pathway, the progressive development of textural and compositional zoning, from a relict core to complex alteration rims, provides valuable records for reconstructing alteration histories and the evolution of their host rock.

In this study, we investigate the Bracco chromitites of the Ligurian Ophiolites (Northern Italy), a rare and possibly unique example of layered chromitites within gabbroic intrusions in a lherzolitic oceanic mantle setting (Bezzi and Piccardo, 1970; Baumgartner et al., 2013). We integrate petrographic, mineralogical, and geochemical analyses to characterize their textures, identify the primary magmatic chromite compositions, and investigate the development of secondary alteration phases, with particular emphasis on chlorite chemistry as a complementary proxy for constraining the alteration conditions. Our aim is to clarify the genetic relationships between magmatic chromite and its alteration products and to reconstruct the sequence of post-magmatic processes, including metamorphic and hydrothermal alteration that have shaped the evolution and preservation of these atypical layered chromitites that are hosted in the mantle sequence of an ophiolite.

2. Geological Background and Sample Descriptions

The Bracco Gabbro Complex spans approximately 12 km² in the Ligurian region of northern Italy, along the Ligurian Sea coast (Figure 1a). It forms part of the Internal Liguride Ophiolites of the Northern Italian Apennines, representing fragments of the Tethyan oceanic domain, formed during the Middle to Upper Jurassic and later exhumed during the Alpine orogeny. The sequence comprises gabbroic intrusions emplaced into mantle peridotites, primarily lherzolite, overlain

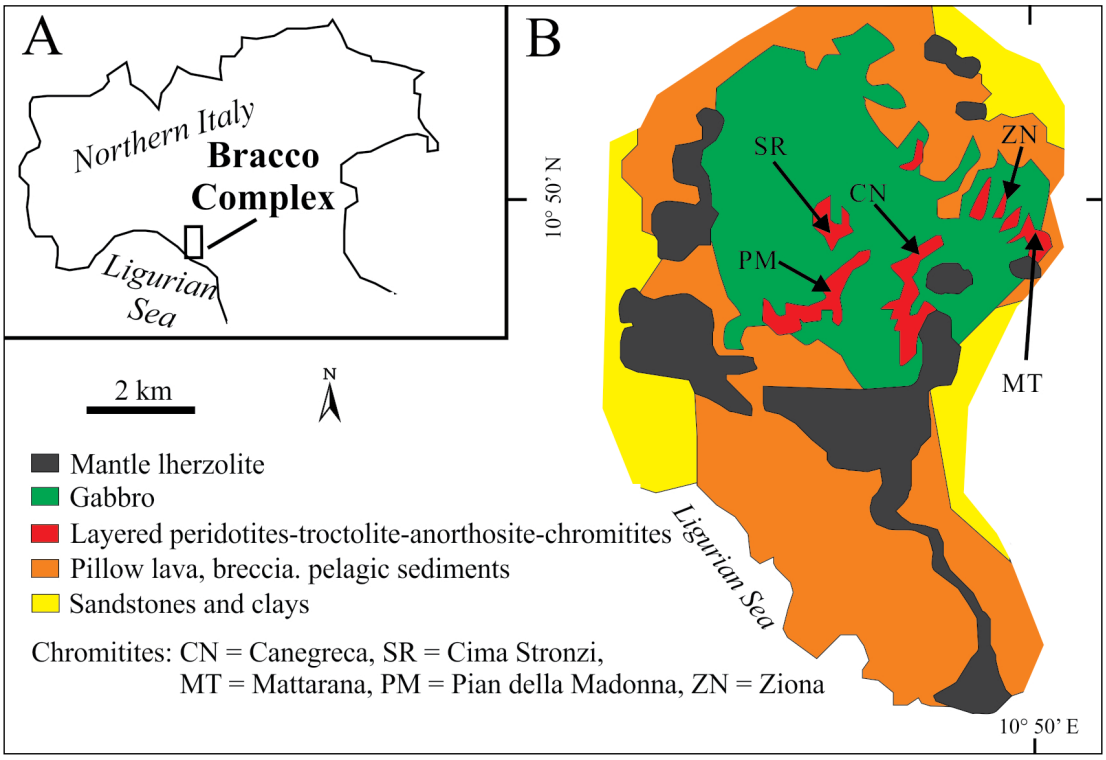

Figure 1- Geographical location; a) and geological map, b) of the Bracco complex, showing the location of our samples.

by mid-ocean ridge (MOR)-affinity basalts and pelagic sediments, including limestones and cherts (Cortesogno et al., 1987; Piccardo et al., 2001). The seafloor cherts host hydrothermal manganese deposits (Cabella et al., 1994). The upper ophiolitic sequence also includes ophicalcite and ophiolitic breccias, formed by seafloor erosion of plutonic and volcanic rocks (Barrett and Spooner, 1977).

Specifically, the Internal Ligurian Ophiolites represent remnants of Jurassic oceanic lithosphere from the Ligurian-Piedmont Ocean, a branch of the Western Tethys Ocean. These ophiolites formed at slowly to ultra-slowly spreading ridges and are among the few preserved examples of subduction-unrelated Mesozoic Tethyan ophiolites in the Mediterranean region. They exhibit features typical of slowly-spreading ridges, including extensive mantle lherzolites and gabbroic intrusions, but with a reduced basaltic crust and scarce sheeted dike complexes (Dilek and Furnes, 2011). The ophiolitic lherzolites are highly serpentinized, and the gabbroic bodies record a polyphase ocean-floor metamorphic evolution, progressing from high- to low-temperature hydrothermal conditions (Cortesogno and Lucchetti, 1984; Cortesogno et al., 1987) reported that the ophiolitic sequence experienced tectono-metamorphic overprinting under prehnite-pumpellyite facies conditions. In contrast, Menna (2009) proposed three metamorphic phases, from granulite- to amphibolite- to greenschist-facies conditions.

The Bracco Gabbro Complex, with an estimated thickness of ~500 meters, was emplaced within fertile mantle lherzolite and comprises gabbroic intrusions accompanied by minor peridotite, troctolite, and anorthosite layers. The complex is in contact with pillow lavas, breccias, and sedimentary rocks, including limestone, chert, sandstone, and clays deposits (Figure 1b). Although the primary mineralogy has been obliterated by metamorphism, the original cumulate textures are well preserved. Chromite occurs as monomineralic pods, veins, ribbon-like bodies, and rhythmic layers (0.1–1 cm thick; Figure 2a, b, c) within troctolite and peridotite at transitional zones adjacent to the main gabbro cumulates (Bezzi and Piccardo, 1970; Baumgartner et al., 2013). Owing to the small size of these mineralized

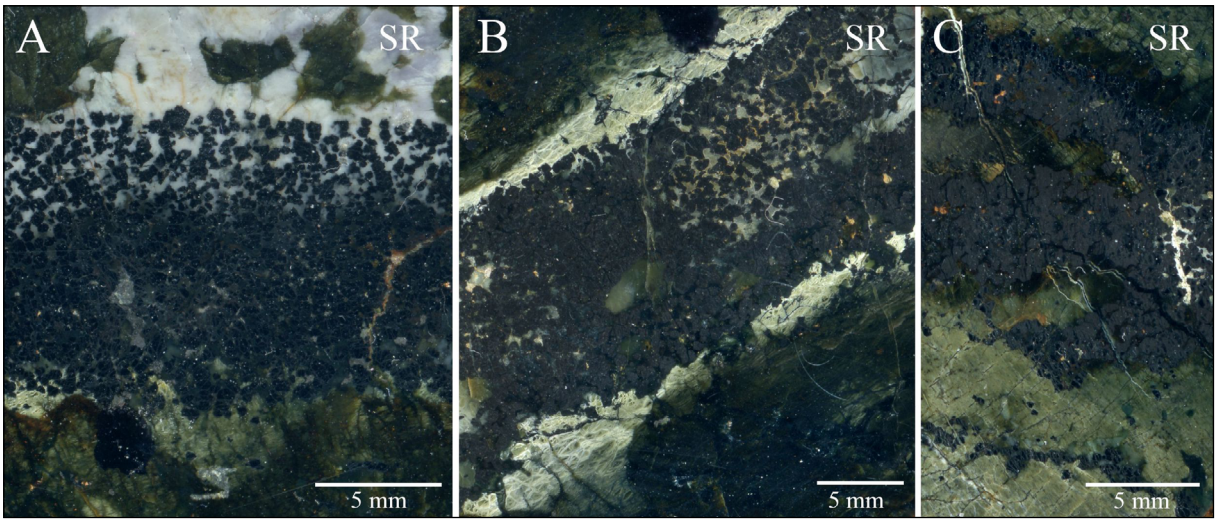

Figure 2- a, b) Hand specimens of the chromitites at the transition between anorthosite and serpentinized peridotite of the Bracco complex, showing the original cumulus textures in thin layers and c) massive texture in a ribbon-like ore. Abbreviation: SR = Cima Stronzi.

bodies, the Bracco chromitites were never mined (Stella, 1924). Samples analyzed in this study were collected from five localities: Canegreca (CN), Cima Stronzi (SR), Mattarana (MT), Pian della Madonna (PM), and Ziona (ZN; Figure 1b).

3. Methods

Spinels and chlorite were analyzed using a JEOL JXA-8200 Electron Probe Microanalyzer (EPMA) in wavelength-dispersive spectrometry (WDS) mode. Analytical conditions included an accelerating voltage of 15 kV, a beam current of 10 nA, and a ~1 μm beam diameter. The Kα emission lines were used to quantify all elements. Calibration was performed with natural and synthetic standards: olivine (Si, Mg), ilmenite (Ti), chromite (Cr), labradorite (Al), vanadium (V), kaersutite (Fe), rhodonite (Mn), wollastonite (Ca), pentlandite (Ni), skutterudite (Co), sphalerite (Zn), albite (Na), and phlogopite (K). Detection limits, calculated automatically by the instrument software and reported in ppm, were: Mg, Mn, Fe, and Co (100); Zn, V, and Ni (150); Cr and Zn (200); Al, Si, Na, K, and Ti (250). The proportions of Fe^{3+} in spinel were calculated assuming ideal spinel stoichiometry. Back-scattered electron (BSE) images and WDS X-ray elemental maps were also acquired with the same instrument. Selected analyses of spinels and chlorite are listed in Tables 1 and 2, respectively.

4. Results

4.1 Textures, Mineralogy, and Mineral Chemistry of Magmatic and Altered Chromitites

Microscopically, the Bracco chromitites exhibit textures ranging from cumulitic and massive to highly disseminated chromite within a serpentine- and chlorite-dominated silicate matrix, with minor relict olivine and clinopyroxene (see Baumgartner et al., 2013).

Chromite grains, ranging in size from a few micrometres up to ~2 mm, display euhedral to lobate and rounded morphologies (Figure 3), and are crosscut by cracks filled with interstitial serpentine and chlorite. Both unaltered and altered chromite grains commonly coexist within the same sample. Most chromite grains show pronounced textural and chemical zoning, characterized by magmatic chromite cores surrounded by (i) an inner rim of relatively homogeneous, porous Fe-Cr oxides (rim 1), dominated by chromian magnetite to ferrian chromite; (see additional details below) and (ii) an outer, more porous, spongy Cr-Fe oxide intergrown with silicates (rim 2), composed of ferrian chromite and subordinate aluminous chromite.

Table 1- Representative analyses of spinels, core and rim, (wt%) from the Bracco chromitites.

Sample	SiO_2	Cr_2O_3	TiO_2	Al_2O_3	FeO	Fe_2O_3	MgO	MnO	K_2O	NiO	ZnO	V_2O_3	CoO	Total
SR core	0.00	32.66	0.84	32.10	19.47	0.61	11.17	0.37	0.00	0.16	0.00	0.12	0.00	97.48
SR core	0.00	32.63	0.01	33.51	15.40	4.58	12.27	0.36	0.76	0.18	0.00	0.08	0.10	99.93
SR core	0.01	32.65	0.12	32.94	16.21	4.24	11.81	0.26	0.82	0.17	0.00	0.22	0.07	99.50
SR core	0.00	32.70	0.12	32.83	16.31	4.81	11.87	0.31	0.78	0.13	0.00	0.10	0.13	100.10
SR core	0.00	32.37	0.14	32.74	16.28	4.63	11.67	0.29	0.78	0.27	0.00	0.08	0.11	99.35
SR core	0.00	32.43	0.04	33.31	15.88	3.32	11.78	0.27	0.78	0.24	0.00	0.11	0.03	98.19
SR core	0.00	33.68	0.12	33.92	16.71	2.86	12.11	0.39	0.66	0.13	0.00	0.14	0.06	100.76
SR core	0.04	34.48	0.12	31.50	17.97	3.43	11.02	0.30	0.57	0.09	0.00	0.17	0.14	99.84
SR core	0.00	34.41	0.07	30.96	17.33	4.06	11.17	0.31	0.63	0.04	0.00	0.19	0.00	99.20
SR core	0.03	33.05	0.17	31.42	17.95	4.19	10.78	0.27	0.64	0.11	0.00	0.13	0.11	98.86
SR core	0.00	33.99	0.14	31.10	17.78	3.60	10.74	0.32	0.64	0.20	0.00	0.29	0.09	98.89
SR core	0.01	35.33	0.17	29.99	18.27	4.54	10.71	0.30	0.59	0.12	0.00	0.09	0.09	100.24
SR core	0.06	32.90	0.57	32.14	19.79	0.59	10.82	0.34	0.00	0.13	0.09	0.13	0.03	97.59
SR core	0.03	32.74	0.62	31.52	19.80	1.73	10.74	0.32	0.00	0.20	0.13	0.12	0.07	98.04
SR core	0.07	32.13	0.69	31.78	19.71	1.19	10.78	0.32	0.00	0.19	0.12	0.12	0.07	97.17
SR core	0.07	32.47	0.78	31.79	19.83	1.27	10.91	0.40	0.00	0.14	0.08	0.14	0.08	97.95
SR core	0.07	32.37	0.82	30.73	20.64	1.32	10.07	0.27	0.00	0.14	0.04	0.11	0.04	96.64
SR core	0.06	33.52	0.76	30.23	20.58	1.82	10.21	0.33	0.00	0.11	0.19	0.11	0.07	98.02
ZN core	0.10	33.63	0.89	32.08	17.93	0.00	11.88	0.29	0.00	0.15	0.04	0.12	0.09	97.21
ZN core	0.13	33.11	0.81	33.17	17.62	0.00	12.41	0.28	0.00	0.19	0.03	0.13	0.04	97.91
ZN core	0.10	32.96	0.71	31.79	17.65	0.36	12.02	0.26	0.00	0.21	0.00	0.12	0.00	96.23
ZN core	0.10	33.54	0.82	32.51	17.53	0.00	12.21	0.25	0.00	0.18	0.05	0.11	0.03	97.33
ZN core	0.06	33.19	0.79	31.88	17.38	0.24	12.29	0.24	0.00	0.18	0.09	0.12	0.11	96.56
ZN core	0.04	33.10	0.79	32.32	17.59	0.19	12.29	0.25	0.00	0.20	0.01	0.14	0.06	97.01
ZN core	0.05	33.52	0.71	32.06	17.46	0.40	12.38	0.26	0.00	0.18	0.04	0.10	0.02	97.22
CN core	0.04	32.64	0.46	33.07	17.69	0.00	11.71	0.31	0.00	0.19	0.01	0.04	0.13	96.32
CN core	0.13	32.77	0.55	33.23	18.86	0.15	11.71	0.27	0.00	0.14	0.10	0.11	0.10	98.11
CN core	0.09	33.06	0.55	33.20	18.06	0.00	12.04	0.24	0.00	0.20	0.02	0.10	0.12	97.66
CN core	0.12	32.40	0.41	33.45	17.60	0.10	12.18	0.32	0.00	0.15	0.11	0.10	0.08	97.04
CN core	0.09	32.82	0.42	33.56	18.58	0.00	11.86	0.22	0.00	0.19	0.00	0.08	0.06	97.87
CN core	0.12	32.70	0.53	33.51	18.55	0.27	11.89	0.31	0.00	0.19	0.05	0.08	0.08	98.29
CN core	0.10	32.76	0.60	33.01	18.60	1.13	12.01	0.31	0.00	0.17	0.08	0.11	0.07	98.94
SR rim	3.79	33.51	0.82	1.82	19.99	25.33	3.66	11.83	0.01	0.12	0.00	0.12	0.00	101.09
SR rim	8.66	33.22	0.85	2.52	24.31	13.46	7.78	7.50	0.00	0.04	0.00	0.09	0.00	98.45
SR rim	3.35	34.97	0.81	1.74	24.92	23.15	2.90	6.83	0.01	0.57	0.00	0.20	0.00	99.52
SR rim	7.46	37.65	0.90	3.82	25.19	8.96	7.01	6.22	0.00	0.00	0.00	0.16	0.00	97.43
SR rim	3.02	36.22	0.09	2.21	20.83	27.22	3.07	8.45	0.90	0.04	0.00	0.29	0.08	102.42
SR rim	4.74	33.96	0.10	2.18	21.84	24.93	4.15	7.71	0.83	0.02	0.00	0.29	0.10	100.92
SR rim	4.64	34.79	0.01	2.17	22.14	25.67	4.08	7.30	0.98	0.00	0.00	0.40	0.09	102.30
SR rim	3.38	38.13	0.13	3.97	20.27	22.68	3.69	9.48	0.74	0.09	0.00	0.26	0.01	102.86
SR rim	3.80	37.71	0.13	4.22	20.43	21.96	4.13	9.48	0.65	0.18	0.00	0.28	0.10	103.07
SR rim	3.56	31.32	0.05	1.95	21.02	31.08	3.03	7.76	1.12	0.05	0.00	0.54	0.04	101.57
SR rim	3.56	30.29	0.04	1.93	20.95	33.00	3.43	7.45	1.22	0.00	0.00	0.51	0.12	102.50
SR rim	3.61	31.68	0.01	2.11	21.24	31.38	3.33	7.80	1.15	0.00	0.00	0.73	0.10	103.11
SR rim	3.39	31.69	0.08	1.94	21.56	31.49	3.23	7.86	0.86	0.00	0.00	0.56	0.12	102.86
SR rim	3.51	29.99	0.12	1.87	21.49	33.27	3.19	7.69	1.01	0.01	0.00	0.55	0.12	102.92
SR rim	3.47	29.93	0.05	1.86	22.02	33.64	3.16	7.68	0.90	0.00	0.00	0.58	0.11	103.47
SR rim	6.61	34.41	0.75	2.54	25.50	16.73	5.63	6.54	0.00	0.16	0.12	0.10	0.06	99.23
SR rim	9.33	31.06	0.85	4.34	24.75	12.59	9.01	5.79	0.00	0.02	0.26	0.03	0.05	98.15
SR rim	8.08	33.09	1.04	4.68	26.11	12.32	7.27	6.08	0.00	0.18	0.16	0.03	0.07	99.15
SR rim	6.21	33.32	1.14	2.52	26.00	17.39	5.18	6.67	0.00	0.03	0.18	0.05	0.00	98.72
SR rim	5.77	32.77	0.77	9.87	25.50	11.11	6.54	5.01	0.00	0.24	0.16	0.13	0.05	97.92
SR rim	7.22	34.18	1.08	3.53	25.86	15.32	6.77	6.29	0.00	0.08	0.29	0.08	0.12	100.83
ZN rim	13.18	23.25	0.44	17.53	13.00	0.00	17.59	0.29	0.00	0.03	0.03	0.05	0.05	85.52
ZN rim	6.67	38.33	0.75	9.17	23.44	4.38	10.30	0.69	0.00	0.07	0.15	0.20	0.05	94.40
ZN rim	8.28	37.51	0.63	9.49	24.36	0.00	11.16	0.52	0.00	0.00	0.07	0.09	0.04	92.12
CN rim	7.09	29.26	0.74	5.39	22.76	17.09	7.12	6.48	0.00	0.67	0.16	0.08	0.10	97.07
CN rim	3.82	33.20	0.96	3.30	22.55	22.82	4.73	7.26	0.00	0.65	0.16	0.13	0.11	99.69
CN rim	5.99	31.54	0.72	4.60	21.81	18.55	7.01	6.78	0.00	0.19	0.22	0.12	0.14	97.75
CN rim	4.53	33.88	0.75	3.78	20.59	22.29	5.51	7.56	0.00	0.15	0.17	0.08	0.09	99.78

Table 2- Representative analyses of chlorite (wt%) associated with the Bracco chromitites.

Sample	SiO_2	TiO_2	Al_2O_3	FeO	MnO	MgO	CaO	Na_2O	K_2O	Cr_2O_3	NiO	Total
CN 1	36.59	0.00	10.37	2.53	0.06	35.88	0.01	0.09	0.02	0.01	0.01	85.57
CN 2	36.96	0.02	9.24	2.88	0.07	37.83	0.02	0.01	0.02	0.04	0.19	87.28
CN 3	37.15	0.00	9.02	2.78	0.01	37.27	0.00	0.02	0.01	0.00	0.15	86.39
CN 4	35.45	0.00	11.81	2.02	0.06	36.54	0.01	0.02	0.03	0.08	0.06	86.07
CN 5	35.09	0.02	12.45	1.90	0.05	34.99	0.05	0.03	0.01	0.21	0.20	84.97
CN 6	29.74	0.00	22.16	1.04	0.00	32.35	0.01	0.02	0.00	0.13	0.08	85.53
CN 7	37.68	0.02	8.24	3.01	0.01	37.92	0.00	0.01	0.01	0.07	0.01	86.97
CN 8	30.11	0.00	20.71	1.12	0.05	32.98	0.00	0.02	0.00	0.85	0.17	86.01
CN 9	29.10	0.00	21.52	1.28	0.00	31.13	0.06	0.02	0.01	1.13	0.38	84.62
CN 10	36.95	0.00	10.21	2.53	0.00	36.72	0.02	0.03	0.02	0.12	0.12	86.73
CN 11	31.29	0.02	19.43	4.50	0.07	29.89	0.15	0.04	0.00	0.24	0.25	85.87
CN 12	32.01	0.00	19.59	1.91	0.03	33.03	0.03	0.00	0.01	0.19	0.09	86.87
CN 13	36.57	0.00	10.64	2.46	0.03	37.47	0.01	0.00	0.00	0.60	0.06	87.85
CN 14	30.37	0.00	21.88	2.26	0.04	32.05	0.04	0.04	0.01	0.35	0.09	87.12
CN 15	30.63	0.02	22.25	1.47	0.05	32.08	0.02	0.06	0.01	0.06	0.03	86.67
CN 16	30.93	0.00	21.93	1.00	0.00	31.97	0.00	0.00	0.00	0.08	0.09	86.00
CN 17	30.85	0.01	20.89	0.86	0.01	31.20	0.01	0.01	0.01	0.17	0.21	84.23
CN 18	31.84	0.00	17.63	1.30	0.01	33.19	0.01	0.03	0.01	0.53	0.01	84.55
CN 19	29.01	0.00	21.60	2.24	0.07	31.51	0.11	0.04	0.02	0.44	0.14	85.19
CN 20	31.63	0.00	19.74	2.46	0.10	32.84	0.14	0.01	0.00	0.11	0.17	87.20
SR 1	32.89	0.02	17.56	5.93	0.46	29.52	0.32	0.07	0.11	0.04	0.10	87.02
SR 2	36.73	0.02	9.56	2.43	0.01	37.06	0.00	0.01	0.00	0.00	0.00	85.84
SR 3	32.08	0.00	18.11	4.50	0.17	31.07	0.11	0.02	0.01	0.04	0.12	86.22
SR 4	35.81	0.00	10.51	3.20	0.04	36.07	0.00	0.00	0.00	0.06	0.09	85.78
SR 5	34.18	0.04	12.07	3.95	0.02	33.91	0.01	0.02	0.00	0.94	0.16	85.31
SR 6	41.13	0.00	0.47	5.43	0.09	39.35	0.01	0.00	0.00	0.00	0.19	86.67
SR 7	40.67	0.01	1.24	4.32	0.00	39.45	0.00	0.00	0.00	0.00	0.32	86.02
SR 8	37.73	0.04	7.38	4.36	0.04	36.02	0.03	0.03	0.03	0.06	0.07	85.78
SR 9	36.24	0.05	9.97	2.43	0.02	36.30	0.02	0.00	0.00	0.05	0.07	85.15
SR 10	33.67	0.06	11.20	13.73	1.18	28.48	0.07	0.02	0.13	0.01	0.07	88.62
SR 11	31.81	0.04	18.26	4.27	0.05	31.35	0.12	0.02	0.00	0.80	0.27	86.99
SR 12	35.08	0.00	16.01	4.86	0.27	31.38	0.12	0.00	0.01	0.02	0.22	87.97
SR 13	31.53	0.01	20.04	3.64	0.03	31.85	0.00	0.01	0.00	0.05	0.16	87.32
SR 14	34.84	0.01	16.48	3.82	0.20	24.35	0.30	0.03	0.05	0.17	0.29	80.54
SR 15	32.40	0.09	18.90	4.19	0.07	30.63	0.06	0.05	0.03	0.28	0.29	86.98
SR 16	32.79	0.06	17.24	6.06	0.32	29.88	0.44	0.17	0.28	0.05	0.14	87.43
SR 17	33.31	0.05	15.75	5.37	0.20	27.67	0.14	0.00	0.03	0.31	0.42	83.24
SR 18	29.78	0.03	20.68	10.08	0.20	27.04	0.01	0.00	0.01	0.05	0.38	88.26
SR 19	27.91	0.03	20.74	13.23	0.10	25.15	0.01	0.02	0.00	2.10	0.23	89.51
SR 20	33.60	0.00	18.04	4.36	0.31	29.84	0.19	0.02	0.01	0.01	0.27	86.64
PM 1	37.84	0.00	7.88	7.92	0.09	32.71	0.06	0.07	0.01	0.00	0.08	86.66
PM 2	36.57	0.01	9.60	8.78	0.13	31.55	0.03	0.09	0.01	0.02	0.12	86.89
PM 3	34.73	0.01	12.70	8.74	0.19	30.30	0.07	0.08	0.02	0.00	0.08	86.91
PM 4	31.97	0.02	17.18	3.07	0.07	28.36	0.03	0.02	0.01	0.36	0.25	81.35
PM 5	32.85	0.01	15.04	8.86	0.26	30.09	0.00	0.02	0.01	0.04	0.15	87.33
PM 6	41.14	0.00	1.51	5.59	0.08	37.81	0.03	0.00	0.00	0.01	0.20	86.36
PM 7	41.43	0.01	1.25	5.53	0.06	37.28	0.01	0.03	0.01	0.01	0.16	85.77
PM 8	35.57	0.00	13.28	8.71	0.23	31.09	0.06	0.01	0.00	0.00	0.05	89.01
PM 9	34.49	0.01	13.13	10.76	0.14	30.05	0.01	0.00	0.01	0.01	0.00	88.60
PM 10	35.65	0.00	12.85	9.16	0.20	30.78	0.03	0.00	0.01	0.00	0.11	88.78
PM 11	34.62	0.02	13.55	2.47	0.10	31.74	0.39	0.02	0.01	0.55	0.04	83.50
PM 12	35.90	0.00	12.81	1.59	0.13	33.31	0.01	0.00	0.01	0.99	0.00	84.75
PM 13	33.53	0.01	15.57	1.89	0.38	32.54	0.03	0.00	0.00	0.11	0.11	84.16
PM 14	33.56	0.00	15.36	1.63	0.23	33.12	0.00	0.00	0.01	0.79	0.09	84.79
PM 15	34.06	0.01	15.11	2.58	0.39	32.67	0.01	0.03	0.01	0.15	0.17	85.19
PM 16	34.44	0.01	14.14	2.36	0.66	32.83	0.02	0.03	0.01	0.10	0.08	84.67
PM 17	33.93	0.02	14.89	1.77	0.15	32.57	0.00	0.02	0.01	0.06	0.13	83.53
PM 18	33.43	0.02	15.85	1.25	0.25	31.50	0.03	0.02	0.00	0.12	0.16	82.63

Table 2- continued.

Sample	SiO_2	TiO_2	Al_2O_3	FeO	MnO	MgO	CaO	Na_2O	K_2O	Cr_2O_3	NiO	Total
PM 19	33.37	0.00	15.94	1.42	0.02	33.03	0.03	0.00	0.02	0.08	0.05	83.95
PM 20	34.07	0.00	13.97	1.56	0.04	31.81	0.06	0.17	0.04	0.03	0.05	81.80
PM 21	34.56	0.01	16.40	2.24	0.13	32.79	0.27	0.05	0.01	0.04	0.04	86.53
PM 22	34.66	0.01	17.25	3.58	0.25	24.69	12.23	0.12	0.11	0.00	0.01	92.91
PM 23	34.24	0.00	16.40	1.69	0.21	32.65	0.23	0.02	0.03	0.00	0.03	85.51
PM 24	34.21	0.00	16.37	1.80	0.19	33.39	0.24	0.05	0.00	0.08	0.00	86.33
PM 25	33.68	0.00	16.88	1.78	0.14	33.78	0.21	0.04	0.00	0.01	0.00	86.52
PM 26	36.19	0.00	13.12	7.23	0.08	29.90	0.79	0.07	0.02	0.00	0.21	87.62
PM 27	37.03	0.00	10.97	2.05	0.16	34.97	0.14	0.05	0.02	0.00	0.00	85.40
PM 28	38.42	0.03	10.37	1.62	0.13	35.06	0.23	0.01	0.00	0.02	0.03	85.93
PM 29	34.70	0.07	15.53	0.95	0.17	30.68	2.10	0.05	0.01	0.00	0.00	84.26
PM 30	31.84	0.08	17.57	1.69	0.18	31.39	0.32	0.07	0.01	0.02	0.00	83.15
ZN 1	37.88	0.01	8.21	5.48	0.27	33.47	0.22	0.02	0.01	0.00	0.14	85.69
ZN 2	38.21	0.00	6.45	7.48	0.11	34.16	0.12	0.00	0.00	0.03	0.00	86.56
ZN 3	37.44	0.02	8.54	7.90	0.11	32.78	0.02	0.02	0.02	0.02	0.01	86.87
ZN 4	39.28	0.02	7.22	7.35	0.10	33.70	0.03	0.02	0.00	0.00	0.05	87.77
ZN 5	35.62	0.01	13.08	1.92	0.17	32.53	0.66	0.04	0.01	0.01	0.13	84.18
ZN 6	38.57	0.00	6.90	6.43	0.11	34.95	0.02	0.04	0.01	0.03	0.02	87.07
ZN 7	32.98	0.00	16.43	7.44	0.59	29.67	0.23	0.02	0.00	0.04	0.13	87.52
ZN 8	36.29	0.01	10.75	6.80	0.23	31.94	0.07	0.04	0.01	0.03	0.05	86.21
ZN 9	36.82	0.00	7.52	7.07	0.10	32.70	0.03	0.06	0.01	0.00	0.01	84.33
ZN 10	35.73	0.02	10.77	6.55	0.23	30.93	0.05	0.05	0.03	0.01	0.06	84.42
ZN 11	36.18	0.04	11.00	2.81	0.33	30.57	0.41	0.08	0.03	0.03	0.26	81.73
ZN 12	37.57	0.01	8.43	5.74	0.07	34.38	0.04	0.03	0.03	0.03	0.01	86.33
ZN 13	38.87	0.03	6.11	4.70	0.05	34.91	0.04	0.06	0.01	0.06	0.03	84.87
ZN 14	37.43	0.03	8.79	7.35	0.17	32.22	0.04	0.08	0.03	0.00	0.06	86.20
ZN 15	38.61	0.02	5.05	4.24	0.11	35.84	0.03	0.06	0.02	0.00	0.07	84.03
ZN 16	38.03	0.05	7.09	5.36	0.04	33.81	0.04	0.06	0.02	0.05	0.00	84.54
ZN 17	37.34	0.01	8.42	5.73	0.12	33.37	0.03	0.09	0.00	0.02	0.06	85.17
ZN 18	35.88	0.03	10.61	6.51	0.18	32.52	0.10	0.04	0.00	0.00	0.10	85.97
ZN 19	36.83	0.01	7.98	6.49	0.17	32.84	0.08	0.04	0.01	0.00	0.09	84.54
ZN 20	36.75	0.00	8.81	7.46	0.19	31.32	0.05	0.07	0.01	0.00	0.05	84.69
ZN 21	28.70	0.00	24.86	1.99	0.00	30.77	0.00	0.01	0.01	0.01	0.06	86.41
ZN 22	27.32	0.00	26.33	1.89	0.02	29.91	0.01	0.00	0.00	0.00	0.06	85.54
ZN 23	29.83	0.00	22.79	2.02	0.00	31.78	0.01	0.00	0.00	0.00	0.04	86.47
ZN 24	30.78	0.01	22.24	2.12	0.02	31.43	0.00	0.00	0.00	0.00	0.03	86.63
ZN 25	34.43	0.00	14.28	8.05	0.12	31.42	0.00	0.03	0.01	0.02	0.00	88.35
ZN 26	30.47	0.00	19.57	2.86	0.00	31.41	0.06	0.00	0.00	0.00	0.00	84.37
ZN 27	34.12	0.01	15.35	7.42	0.10	31.23	0.01	0.00	0.00	0.01	0.03	88.28
ZN 28	33.00	0.00	17.72	4.84	0.13	31.81	0.04	0.09	0.00	0.05	0.02	87.71
ZN 29	29.42	0.03	23.30	2.18	0.00	31.20	0.00	0.11	0.00	0.03	0.10	86.37
ZN 30	29.89	0.00	23.11	2.05	0.00	31.51	0.05	0.06	0.01	0.03	0.08	86.77
ZN 31	30.44	0.02	22.60	2.06	0.04	31.86	0.02	0.06	0.00	0.00	0.02	87.12
ZN 32	30.84	0.00	20.22	2.00	0.00	32.19	0.00	0.01	0.00	0.03	0.03	85.32
ZN 33	29.13	0.02	22.42	2.10	0.01	31.23	0.02	0.00	0.00	0.04	0.08	85.04
ZN 34	29.32	0.02	22.45	1.73	0.03	31.25	0.15	0.08	0.01	0.10	0.00	85.13
ZN 35	27.19	0.00	27.48	1.25	0.01	30.03	0.00	0.09	0.01	1.86	0.09	88.01
ZN 36	29.40	0.00	20.47	1.90	0.07	31.37	0.01	0.00	0.00	2.71	0.11	86.04
ZN 37	26.68	0.00	26.12	1.55	0.05	29.90	0.04	0.00	0.00	0.01	0.01	84.36
ZN 38	29.39	0.00	22.69	1.28	0.00	32.01	0.00	0.01	0.00	0.02	0.05	85.45
ZN 39	31.94	0.00	18.50	2.23	0.06	32.51	0.00	0.00	0.01	0.58	0.09	85.93
ZN 40	30.71	0.08	20.73	3.03	0.04	31.67	0.00	0.03	0.00	1.98	0.32	88.59
ZN 41	31.00	0.00	19.81	2.16	0.06	31.75	0.03	0.02	0.00	0.07	0.06	84.95
ZN 42	30.64	0.01	21.51	1.27	0.00	32.20	0.02	0.04	0.00	0.14	0.01	85.82
ZN 43	28.82	5.46	19.77	1.58	0.00	30.50	0.02	0.05	0.01	1.02	0.13	87.36
ZN 44	29.37	0.01	22.42	1.05	0.00	32.45	0.00	0.04	0.00	0.02	0.03	85.38
ZN 45	31.47	0.02	20.06	1.42	0.06	32.58	0.00	0.01	0.00	0.02	0.18	85.82
ZN 46	30.49	0.00	22.00	1.09	0.03	32.00	0.00	0.00	0.00	0.08	0.13	85.82

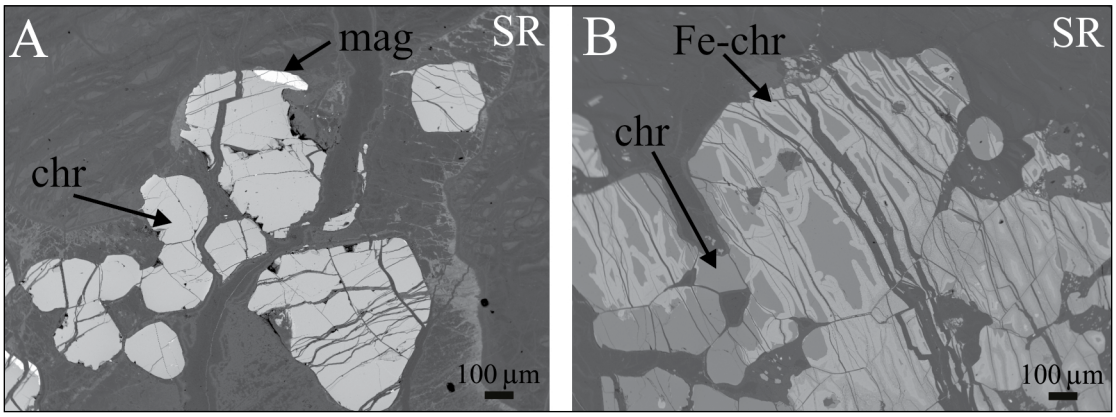

Figure 3- BSE images of polished sections, showing the microscopic textures of the Bracco chromitite, a) Euhedral, lobate and rounded unaltered chromite grains only partially transformed in magnetite, b) co-existence of partially- to totally-altered, and fresh chromite grains. The altered silicates consist of serpentine and chlorite. Abbreviations: chr = chromite, Fe-chr = ferrian chromite, mag = magnetite, SR = Cima Stronzi.

Back-scattered electron imaging reveals that rim 2 commonly displays oscillatory fine-scale banding, with alternating relatively homogeneous and distinctly spongy, silicate-enriched bands containing abundant chlorite. Both rim 1 and rim 2 alteration features are consistently observed across all chromitite samples, although some grains exhibit only the rim 2 alteration type.

Electron probe microanalysis shows that the major oxide ranges (wt%) in chromite cores from this study align with and complement those reported by Baumgartner et al. (2013) and Zaccarini et al. (2025): Cr_2O_3 = 29.63–39.87, Al_2O_3 = 20.28–37.34, MgO = 11.38–17.34, FeO = 11.38–22.77, Fe_2O_3 = 1.33–8.12, TiO_2 = 0.41–1.12, and MnO = 0.21–0.39, with SiO_2, ZnO, CoO, V_2O_3, and NiO typically below 0.2 wt%.

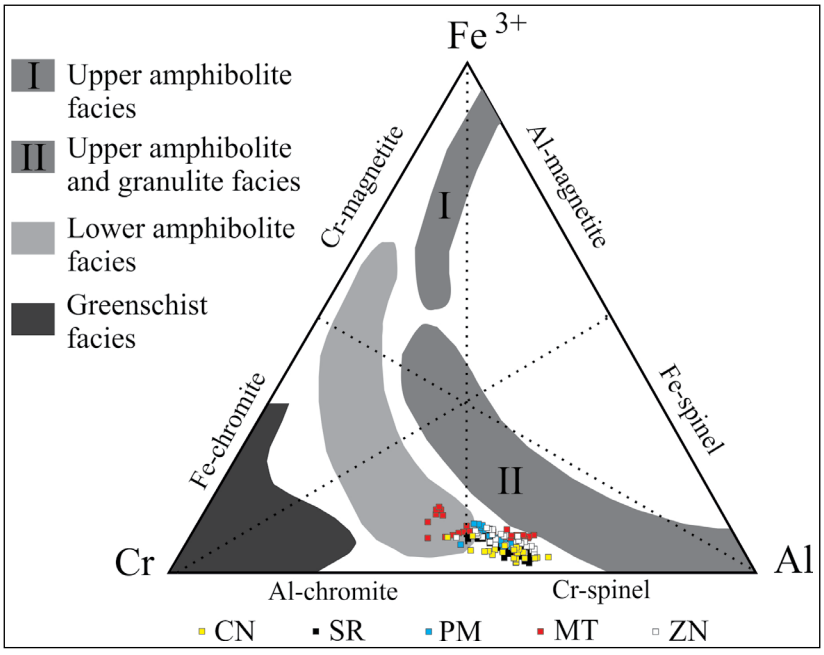

Figure 4- The composition of chromite in the Bracco complex plotted in the Cr–Al–Fe^{3+} diagram (Stevens, 1944). The spinel compositional fields from different metamorphic facies are from Purvis et al. (1972), Evans and Frost (1975) and De Freitas Suita, and Strieder (1996). Abbreviations: CN = Canegreca, SR = Cima Stronzi, PM = Pian della Madonna, MT = Mattarna, ZN = Ziona.

In Stevens' (1944) Cr–Al–Fe^{3+} classification diagram (Figure 4), most data plot in the chromian spinel field, with a few in the aluminous chromite field. The spinel cores are Fe^{3+}-poor and relatively Al-rich, with Cr# values of 0.34–0.56, consistent with previous studies. Comparison with Cr–Al–Fe^{3+} fields in metamorphic spinels (Purvis et al., 1972; Evans and Frost, 1975; De Freitas Suita and Strieder, 1996; Figure 4) further indicates a largely preserved magmatic composition, with most compositions falling well outside the greenschist- and amphibolite-facies fields.

X-ray elemental maps, spot analyses, and transects resolve marked compositional variations from magmatic chromite cores to altered rims (rims 1 and 2; see above). Paired core and rim analyses plotted in the Cr–Al–Fe^{3+} diagram (Figure 5) show that chromite cores fall in the chromian spinel field with low Fe^{3+} contents, whereas altered rims, particularly rim 1 are Fe^{3+}-rich, plotting at the boundary between ferrian chromite and chromian magnetite. In contrast, rim 2 shows lower Fe^{3+} proportions, spanning from aluminous chromite into the ferrian chromite field. Transect analyses across partially altered chromite grains (Figure 6 a-d and 7 a, b) reveal a homogeneous magmatic core, whereas rims are generally marked by distinct Al and Mg depletions and relative enrichments in Cr, Fe^{2+}, Fe^{3+}, Mn, and Si. Rim 1, where present, shows higher Fe^{3+} contents than rim 2, with Fe^{2+} levels remaining at the same level (Figure 6 a, b and 7 a). Although rim 2 is dominated by Fe-chromite (Figure 5), Cr contents oscillate strongly owing to fine-scale bands containing abundant Cr-poor silicate inclusions (Figures 6 a-d, 7 a, b). Rare, altered chromite grains exhibit strong Mn enrichment at the interface between preserved cores and rim 2 (Figures 6 a-d and 7). Entirely altered chromite grains typically lack distinct chemical patterns (Figure 7 a, b).

The BSE image and the element-distribution maps also show the complexity of the internal texture of the altered spinel grains and the consistent presence of Cr, Al, Fe, Mg, Si, Mn and Ti (Figure 8).

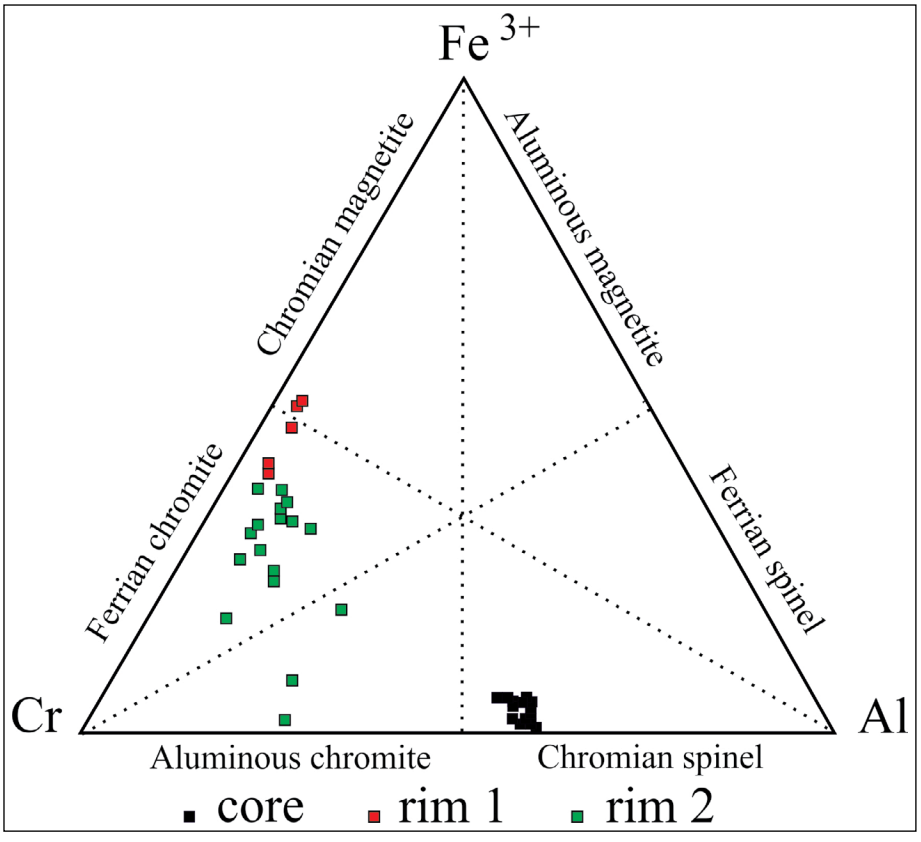

Figure 5- Ternary Cr–Al–Fe^{3+} diagram showing the different compositions among the magmatic core and the altered rims (1 and 2) in the Bracco chromitites.

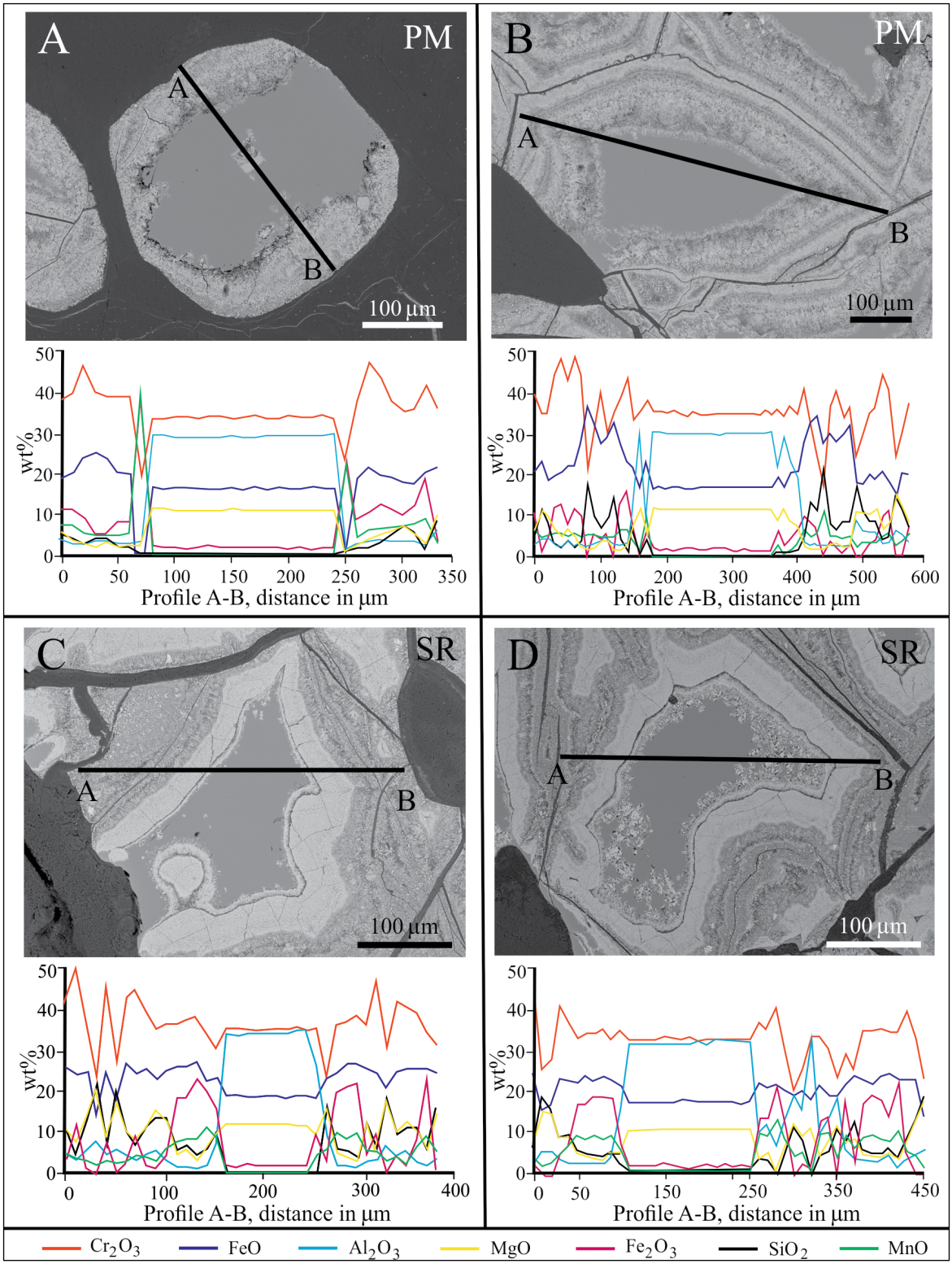

Figure 6- BSE images and chemical variation across the chromite core (fresh chromite) to altered rims (profiles A-B) in the Bracco chromitites. Samples from Pian della Madonna and from Cima Stronzi. Abbreviations: SR = Cima Stronzi, PM = Pian della Madonna.

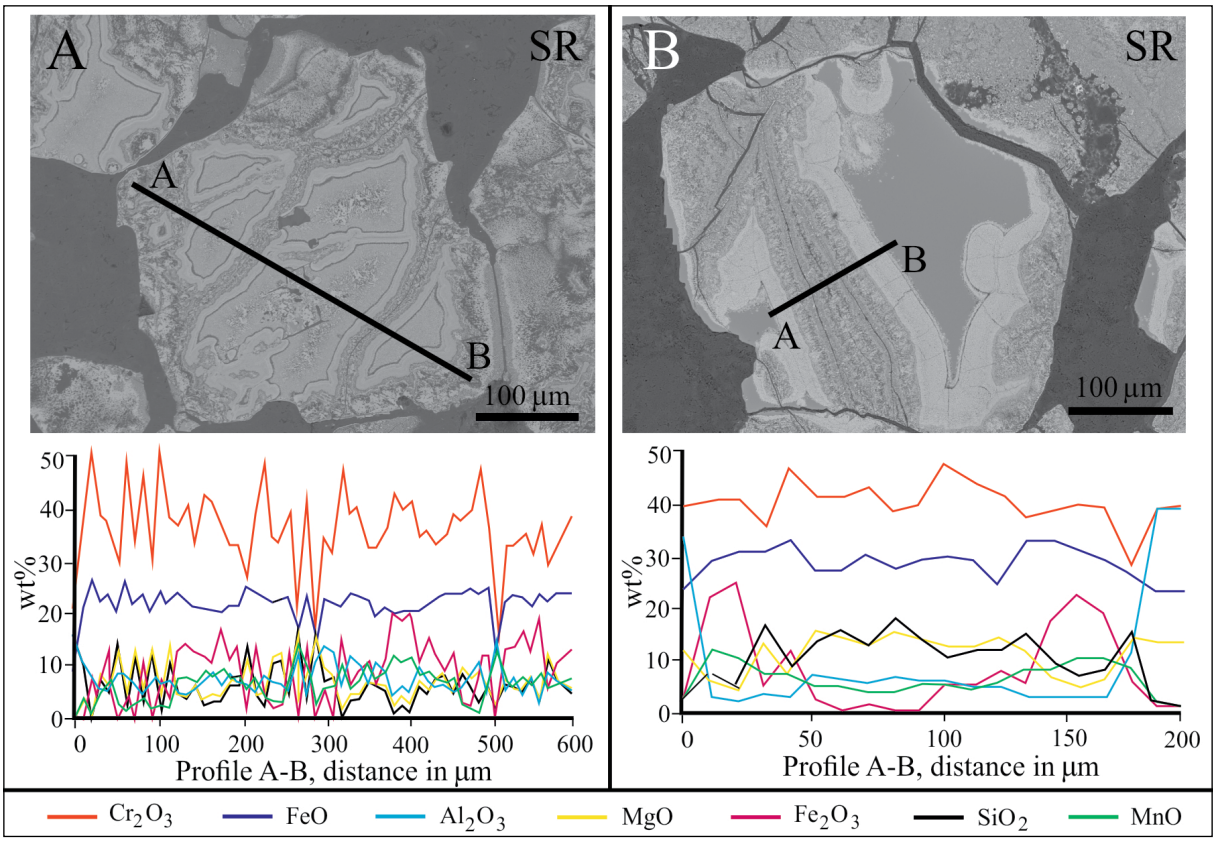

Figure 7- a) BSE images and chemical variation across a totally altered grain of chromite and b) across the altered rims, (profiles A-B) in the Bracco chromitites. Abbreviation: SR = Cima Stronzi.

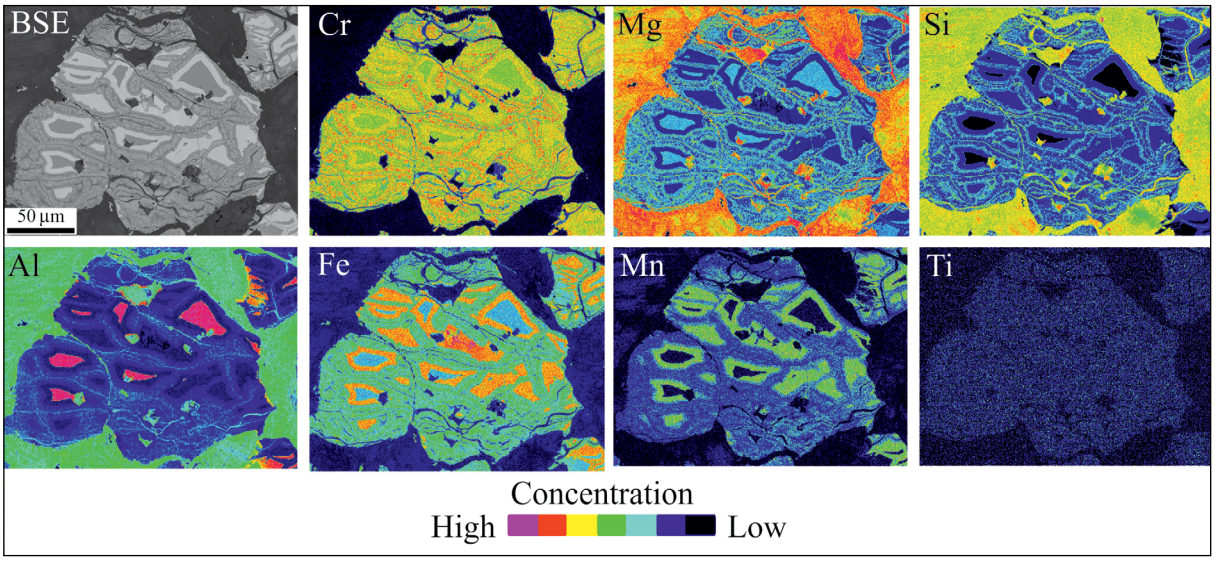

Figure 8- BSE image and X-ray element-distribution maps of Cr, Al, Fe, Mg, Si, Mn and Ti of a partially to totally altered grain of chromite from the Bracco chromitites. Abbreviation: SR = Cima Stronzi.

4.2. Chlorite Chemistry and Thermometry

The chemical compositions of chlorite associated with chromite-alteration rims in the analyzed Bracco chromitites are presented as plots of Fe versus Si variation (Figure 9a) in the diagram proposed by Hey (1954). According to the nomenclature provided by Bayliss (1975), the chlorites are identified as clinochlore. The compositional range is primarily controlled by the contents of Si (26.68–39.28 wt% SiO_2) and Fe (0.86-13.73 wt% FeO_{tot}), corresponding to ~5-7.5 and 0.1-1.7 atoms per formula unit (a.p.f.u.), respectively. Other major element values are highly variable, with Al_2O_3 ranging from 6.45 to 27.48 wt%, and MgO from 24.35 to 37.92 wt%. Notably, Cr_2O_3 reaches up to 2.71 wt%, whereas MnO, CaO, Na_2O, K_2O, and NiO are consistently below 0.2 wt%.

Chlorite mineral chemistry can provide insights into its formation conditions (Cathelineau and Nieva, 1985; Kranidiotis and McLean, 1987; Cathelineau, 1988; Zang and Fyfe, 1995). Although De Caritat et al. (1993) noted that host rock composition can influence the thermodynamic interpretation of chlorite data, it has been shown that the degree of tetrahedral Al (^{IV}Al) substitution for Si is primarily dependent

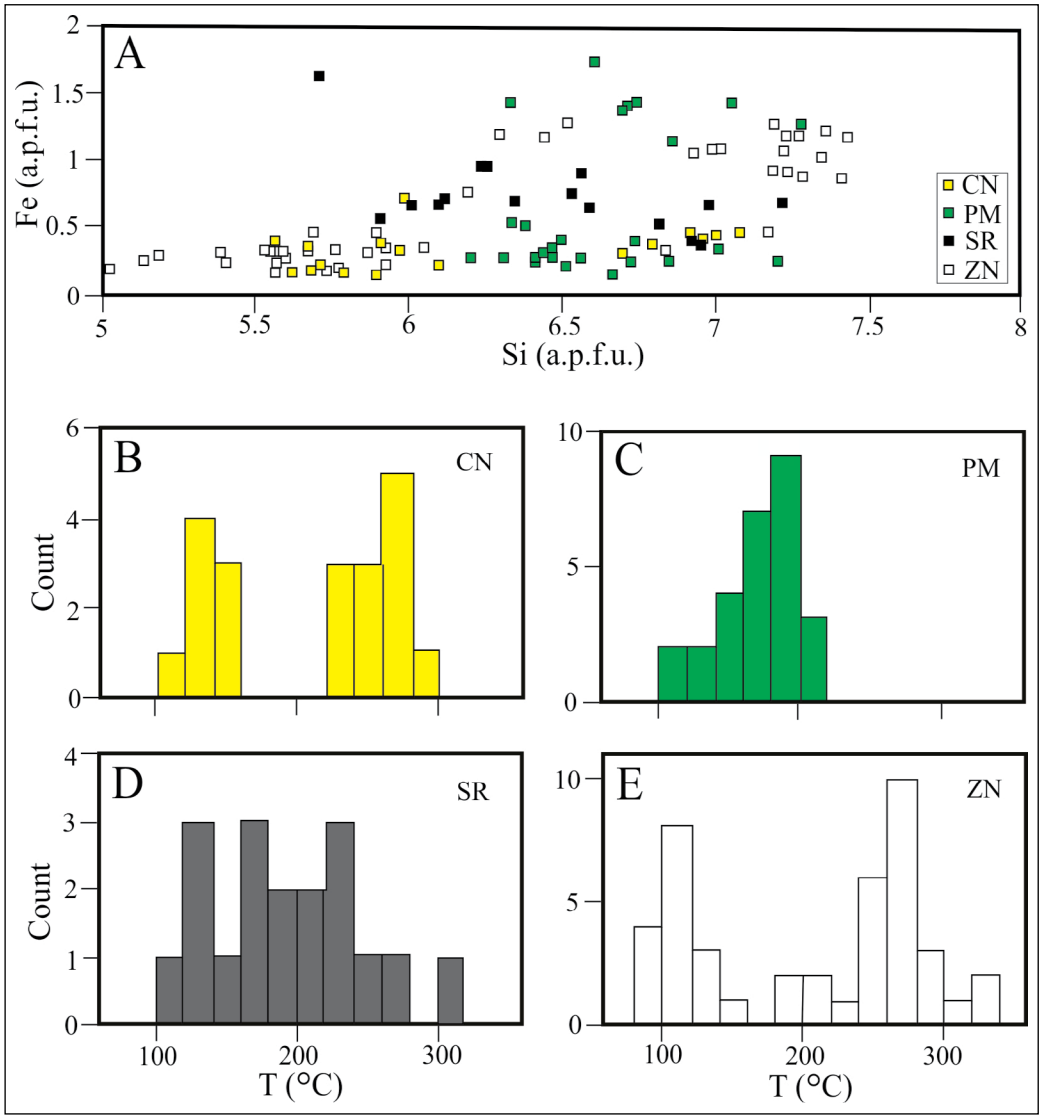

Figure 9- a) Plot of compositions of chlorite from Bracco chromitites on diagram Fe (a.p.f.u.) versus Si (a.p.f.u.) (modified after Hey, 1954) and b, c, d, e) statistics of chlorite geothermometry based on the equation of Kranidiotis and MacLean (1987). Abbreviations: CN = Canegreca, PM = Pian della Madonna, SR = Cima Stronzi, ZN = Ziona.

on thermal conditions, increasing with higher precipitation temperatures (Cathelineau and Nieva, 1985; Kranidiotis and McLean, 1987; Cathelineau, 1988; Zang and Fyfe, 1995). Application of the Kranidiotis and McLean (1987) geothermometer yields temperatures ranging from 86 to 334 °C across all samples (Figure 9b-e).

Distinct differences in the Si (a,p.f.u.) content in chlorite (Figure 9 a) and inferred formation temperatures are evident among chromitite localities investigated. At PM, calculated temperatures show a narrow range of 100–200 °C, with most values clustering near 200 °C (Figure 9 c). In contrast, SR exhibits a broader temperature range of 100–300 °C, with higher-temperature chlorite (>250 °C), (Figure 9 d). Similarly, chlorite from CN and ZN indicate formation at ~100–300 °C, with most values clustering around 280 °C (Figure 9 b, e).

5. Discussion

Chromite is among the most alteration-resistant magmatic minerals, typically retaining its primary composition even through metamorphism. Fully metamorphosed chromitites lacking any magmatic signature are rare and largely restricted to Precambrian examples (Fleet et al., 1993; Proenza et al., 2008; Portella et al., 2016). Similarly, the Bracco chromitites exhibit only partial replacement of primary chromite, preserving magmatic chromite cores surrounded by complex alteration zones, including: (i) an inner rim (rim 1) of relatively homogeneous, Fe^{3+}-rich ferrian chromite, and (ii) an outer rim (rim 2) of comparatively Fe^{3+}-poor, Cr-rich ferrian chromite, intimately associated with abundant silicate inclusions, particularly chlorite.

This alteration pattern closely parallels other examples of metamorphic–hydrothermal alteration in ophiolite-hosted chromitites worldwide, characterized by partial to extensive chromite replacement and the development of zoned textures comprising a magmatic chromite core, a ferrian chromite corona and, finally, porous chromite filled with secondary phases, especially chlorite (Tarkian et al., 1992; Mellini et al., 2005; Garuti et al., 2007, 2012; Merlini et al., 2009; Gervilla et al., 2012; Grieco and Merlini, 2012; Bussolesi et al., 2022; Sideridis et al., 2022; Garcia-Casco et al., 2025). During the chromite alteration in the presence of an aqueous fluid, Al and Mg are released from the magmatic spinel resulting in the formation of ferrian chromite and chlorite through the following reaction (Kimball, 1990):

$$MgAl_2O_4 + 4MgO + 3SiO_2 + 4H_2O = Mg_5AlAlSi_3O_{10}(OH)_8,$$

with SiO_2, H_2O and part of the MgO introduced from a fluid phase. The fluids responsible for the alteration of chromite and precipitation of chlorite are hydrothermal in origin, generally formed at low temperature during oceanic serpentinization, weathering and lateritization processes (Tarkian et al., 1992; Mellini et al., 2005; Garuti et al., 2007; Merlini et al., 2009; Grieco and Merlini, 2012; Bussolesi et al., 2022; Sideridis et al., 2022) or formed at higher temperatures during prograde metamorphism (Merlini et al., 2009; Gervilla et al., 2012).

Grieco and Merlini (2012) suggested that the formation of ferrian chromite and chlorite in the Vourinos chromitites likely initiated at >300 °C, prior to serpentinization, but continued to lower temperatures within the serpentinization field, driven by externally introduced, Si-rich and potentially oxidizing fluids infiltrating along fractures. These fluids maintained sufficient silica activity to promote chromite alteration under conditions of chemical disequilibrium with the surrounding serpentinite. The coexistence of fresh and intensely altered chromite grains at centimeter to millimeter scales, with some chromite fully replaced by rim 1 and rim 2 assemblages (Figures 3 a, b, 6 a-d, 7 a, b), attests to localized fluid infiltration and heterogeneous alteration pathways, sustaining disequilibrium alteration alongside serpentinization.

Thermometry calculations for chlorite provide further constraints: the presence of clinochlore in most Bracco chromitites indicates alteration temperatures up to ~330 °C, whereas calculated temperatures as low as ~100 °C or below suggest the presence of talc-chlorite mixed-layer phase (Figure 9 a-e). Distinct thermometric peaks at ~280 °C and ~100–150 °C provide additional evidence for retrograde evolution, likely involving multiple fluid pulses. These events likely facilitated the formation of the two texturally, mineralogically, and chemically distinct rim 1 and rim

2 assemblages surrounding preserved chromite cores (Figures 3a, b, 6 a-d, 7 a, b).

Notably, the altered chromite rims, particularly rim 1 mantling fresh chromite cores, are strongly enriched in MnO relative to magmatic chromite. This enrichment is accompanied by an increase in Fe_2O_3/FeO ratios from unaltered chromite (0.06–0.29 wt%) to altered rims (0.19–1.17 wt%), with rim 1 exhibiting higher Fe^{3+} contents than rim 2 (Figure 5). These chemical signatures suggest progressive oxidation during alteration, with the Mn-rich rim 1 representing a later alteration stage that advanced inward, progressively replacing and overprinting both the chromite cores and earlier-formed rim 2 through continued recrystallization and oxidation. Similar MnO enrichment has been documented in other ophiolitic chromitites, with contents reaching up to 14.4 wt% in strongly altered podiform chromitites in northern Greece (Paraskevopoulos and Economou, 1981; Grieco and Merlini, 2012). In the Bracco chromitites, this Mn enrichment likely reflects infiltration of Mn-bearing, seawater-rich hydrothermal fluids, perhaps comparable to those responsible for seafloor hydrothermal Mn deposits in the Ligurian ophiolites (Cabella et al., 1994).

Collectively, the mineralogical, chemical, and textural features imply that chromite alteration in the Bracco chromitites reflects a multi-stage, fluid-mediated process, initiated at relatively high temperatures (>300 °C) and evolving under decreasing temperatures and variable redox conditions during serpentinization. The MnO enrichment and progressive oxidation point to hydrothermal circulation in a still-warm oceanic lithosphere, similar to alteration processes documented in the Vourinos complex (Grieco and Merlini, 2012). Fluid flow was likely controlled by a network of fractures, enabling seawater-derived, oxidizing, silica- and Mn-rich fluids to infiltrate a shallow lithospheric environment, driving metasomatic alteration and the development of the observed alteration rims.

6. Concluding Remarks

In this contribution, the composition of magmatic and altered chromites, combined with chlorite geothermometry in the Bracco chromitites of the Ligurian ophiolites have been used to better understand both their magmatic and post-magmatic evolution, as well as that of their host rocks. The results confirm that the Bracco chromitites display distinctive characteristics: although spatially associated with gabbroic intrusions within oceanic lithosphere formed at slowly- to ultra-slowly spreading ridges, their layered cumulate texture and chemical composition are more typical of stratiform chromitites formed in stable cratonic settings.

Following magmatic crystallization, the Bracco chromitites underwent alteration driven by interaction with hydrothermal fluids. This metamorphic alteration led to significant chemical modification of chromite and the formation of secondary phases, including ferrian chromite and chlorite. Textural observations, chemical analyses, and chlorite thermometry yielding temperatures from well above 300 °C to below 100 °C collectively point to a genetic link with fluid-driven oceanic alteration, with calculated temperatures remaining within prehnite-pumpellyite facies conditions.

The fluids responsible for chromite alteration were hydrothermal in origin, circulating through fracture networks within a still-warm oceanic lithosphere at relatively shallow depths. These fluids were locally oxidizing, dominated by seawater, and enriched in SiO_2 and MnO. The enrichment of MnO in altered chromite suggests a possible connection between the hydrothermal fluids responsible for chromite alteration and those that formed seafloor Mn deposits reported in the Ligurian ophiolites. In this context, we propose that the Bracco chromitites and their associated lherzolitic mantle were at least partially exposed at the Tethyan seafloor and underwent low-temperature hydrothermal alteration prior to the orogenic emplacement of their ophiolite host.

Acknowledgments

We are grateful to Robert Martin, an anonymous reviewer and the editor, whose comments greatly improved the quality of the manuscript. We also acknowledge Sinan Akiska for his invitation to contribute to the special issue in Memory of Prof. Taner Ünlü.

References

Arai, S., Uesugi, J., Ahmed, A. H. 2004. Upper crustal podiform chromitite from the northern Oman ophiolite as the stratigraphically shallowest chromitite in ophiolite and its implication for Cr concentration. Contributions to Mineralogy and Petrology 147, 145–154.

Barnes, S. J. 2000. Chromite in komatiites, II. Modification during greenschist to mid-amphibolite facies metamorphism. Journal of Petrology 41, 387–409.

Barnes, S. J., Roeder, P. L. 2001. The range of spinel compositions in terrestrial mafic and ultramafic rocks. Journal of Petrology 42, 2279–2302.

Barrett, J. J, Spooner, E. F. C. 1977. Ophiolitic breccias associated with allochthonous oceanic crustal rocks in the East Ligurian Apennines, Italy—A comparison with observations from rifted oceanic ridges. Earth Planetary Science Letters 35, 79–91.

Baumgartner, R. J., Zaccarini, F., Garuti, G., Thalhammer, O. A. R. 2013. Mineralogical and geochemical investigation of layered chromitites from the Bracco-Gabbro complex, Ligurian ophiolite, Italy. Contribution to. Mineralogy and Petrology 165, 477–493.

Bayliss, P. 1975. Nomenclature of the trioctahedral chlorite. Canadian Mineralogist 13, 178–180.

Bezzi, A., Piccardo, G. B. 1970. Studi petrografici sulle formazioni ofiolitiche della Liguria. Riflessioni sulla genesi dei complessi ofiolitici in ambiente appenninico e alpino. Rendiconti della Societa Italiana di Mineralogia e Petrologia 26, 1-42.

Bliss, N. W., MacLean, W. H. 1975. The paragenesis of zoned chromite from central Manitoba. Geochimica et Cosmochimica Acta 39, 973–990.

Bosi, F., Biagioni, C., Pasero, M. 2019. Nomenclature and classification of the spinel supergroup. European Journal of Mineralogy, 31, 183–192.

Boudier, F., Al-Rajhi, A. 2014. Structural control on chromite deposits in ophiolites: The Oman case. In Tectonic Evolution of the Oman Mountain; Special Publications; Rollinson, H.R., Searle, M.P., Abbasi, I.A., Al-Lazki, A., Al Kindi, M.H., Eds.; The Geological Society of London: London, UK, 392, 259–273.

Burkhard, D. J. M. 1993. Accessory chromium spinels: Their coexistence and alteration in serpentinites. Geochimica et Cosmochimica Acta 57, 1297–1306.

Bussolesi, M., Grieco, G., Zaccarini, F., Cavallo, A., Tzamos, E., Storni, N. 2022. Chromite compositional variability and associated PGE enrichments in chromitites from the Gomati and Nea Roda ophiolite, Chalkidiki, Northern Greece. Mineralium Deposita 57, 1323–1342.

Cabella, R., Cortesogno, L., Gaggero, L. 1994. Hydrothermal contributions to cherts deposition in Northern Apennines: a preliminar report. Ofioliti 19, 367–376.

Cathelineau, M. 1988. Cation site occupancy in chlorites and illites as a function of temperature. Clay Mineral 23, 471–485.

Cathelineau, M., Nieva, D. 1985. A chlorite solid solution geothermometer. The Los Azufres (Mexico) geothermal system. Contribution to Mineralogy and Petrology 91, 235–244.

Cortesogno, L., Lucchetti, G. 1984. Ocean floor metamorphism of the volcanic and sedimentary sequences in the Northern Apennine ophiolites: mineralogical and paragenetic features. Ofioliti 9, 363-400.

Cortesogno, L., Galbiati, B., Principi, G. 1987. Note alla "Carta geologica delle ofioliti del Bracco" e ricostruzione della paleogeografia Giurassico, Cretacica. Ofioliti, 12, 261–342.

De Caritat P., Hutcheon, I., Walshe, J. L. 1993. Chlorite geothermometry: a review. Clays Clay Minerals 41, 219–239.

De Freitas Suita, M. T., Strieder, A. J. 1996. Cr-spinels from Brazilian mafic–ultramafic complexes: Metamorphic modifications. International Geology Reviews 38, 245–267.

Dick, H. J. B., Bullen, T. 1984. Chromian spinel as a petrogenetic indicator in abyssal and alpine-type peridotites and spatially associated lavas. Contribution to. Mineralogy and Petrology 86, 54–76.

Dilek, Y., Furnes, H. 2011. Ophiolite genesis and global tectonics: Geochemical and tectonic fingerprinting of ancient oceanic lithosphere. Geological Society of America Bulletin. 123, 387–411.

Evans, B. W., Frost, B. R. 1975. Chome-spinel in progressive metamorphism — A preliminary analysis. Geochimica Cosmochimica Acta 39, 959–972.

Fleet, M. E., Angeli, N., Pan, Y. 1993. Oriented chlorite lamellae in chromite from the Pedra Branca mafic-ultramafic complex, Ceari, Brazil. American Mineralogist 78, 68–74.

Garcia-Casco, A., Pujol-Solà, N., Novo-Fernández, I., Arenas, R., Rojo-Pérez, E., Cambeses, A., Molina, J. F., Sánchez Martínez, S., Domínguez-Carretero,

D., Iglesias, G., Proenza, J. A. 2025. General conceptual petrological model for the subsolidus transformation of chromitite with application and implications, Journal of Petrology 66.

Garuti, G., Proenza, J. A., Zaccarini, F. 2007. Distribution and mineralogy of platinum-group elements in altered chromitites of the Campo Formoso layered intrusion (Bahia State, Brazil): control by magmatic and hydrothermal processes. Mineralogy and Petrology 89, 159–188.

Garuti, G., Zaccarini, F., Proenza, J. A., Thalhammer, O. A. R., Angeli, N. 2012. Platinum-group minerals in chromitites of the Niquelândia Layered Intrusion (central Goias, Brazil): their magmatic origin and low-temperature reworking during serpentinization and lateritic weathering. Minerals 2, 365-384.

Gervilla, F., Padron-Navarta J. A., Kerestedjian, T., Sergeeva, I., Gonzalez-Jimenez, J. M., Fanlo, I. 2012. Formation of ferrian chromite in podiform chromitites from the Golyamo Kamenyane serpentinite, Eastern Rhodopes, SE Bulgaria: a two-stage process. Contribution to Mineralogy and Petrology 164, 643–657.

Grieco, G., Merlini, A. 2012. Chromite alteration processes within Vourinos ophiolite. International Journal of Earth Sciences 101, 1523–1533.

Hey, M. H. 1954. A new review of the chlorites. Mineral Mag 30, 277–292.

Irvine, T. N. 1965. Chromian spinel as a petrogenetic indicator: Part 1. Theory. Canadian Journal of Earth Sciences 648–672.

Kamenetsky, V. S., Crawford, A. J., Meffre, S. 2002. Factors controlling chemistry of magmatic spinel: An empirical study of associated olivine, Cr-spinel and melt inclusions from primitive rocks. Journal of Petrology 42, 655–671.

Kimball, K. L. 1990. Effects of hydrothermal alteration on the composition of chromian spinels. Contribution to Mineralogy and Petrology 105, 337–346.

Kranidiotis, P., MacLean, W. H. 1987. Systematic of chlorite alteration at the Phelps Dodge massive sulfide deposit, Matagami, Quebec. Economic Geology 82, 1898–1911.

Leblanc, M., Nicolas, A. 1992. Ophioliticchromititites International Geology Review 34,653–686.

Loferski, P. J. 1986. Petrology of metamorphosed chromite-bearing ultramafic rocks from the Red Lodge District, Montana. Contributions to the geology of mineral deposits. U.S. Geological Survey Bulletin, 1626-B.

Mellini, M., Rumori, C., Viti, C. 2005. Hydrothermally reset magmatic spinels in retrograde serpentinites, formation of “ferritchromit” rims and chlorite aureoles. Contributions to Mineralogy and Petrology 149, 266–275.

Merlini, A., Grieco, G., Diella, V. 2009. Ferritchromite and chromian-chlorite formation in mélange-hosted Kalkan chromitite (Southern Urals, Russia). American Mineralogist 94, 1459–1467.

Menna, F. 2009. From magmatic to metamorphic deformations in a Jurassic ophiolitic complex: the Bracco gabbroic massif, eastern Liguria (Italy), Ofioliti 34, 109–130.

Paraskevopoulos, G. M., Economou, M. 1981. Zoned Mn-rich chromite from podiform type chromite ore in serpentinites of northern Greece. American Mineralogist 66, 1013–1019.

Piccardo, G. B., Rampone, E., Romairone, A., Scambelluri, M., Tribuzio, R., Beretta, C. B. 2001. Evolution of the Ligurian Tethys: inference from petrology and geochemistry of the Ligurian Ophiolites. Periodico di Mineralogia 70, 147–192.

Portella, Y. D. M., Zaccarini, F., Luvizotto, G. L., Garuti, G., Bakker, R. J., Angeli, N., Thalhammer, O. 2016. The Cedrolina chromitite, Goiás State, Brazil: a metamorphic puzzle. Minerals 6, 91.

Proenza, J. A., Zaccarini, F., Escayola, M., Cábana, C., Schalamuk, A., Garuti, G. 2008. Composition and textures of chromite and platinum-group minerals in chromitites of the western ophiolitic belt from Pampean Ranges of Córdoba, Argentina. Ore Geology Reviews 33, 32–48.

Purvis, A. C., Nesbitt, R. W., Hallberg, J. A., 1972. The geology of part of the Carr Boyd Complex andits associated nickel mineralization, Western Australia. Economic Geology 67 1093–1113.

Sideridis, A., Tsikouras, B., Tsitsanis, P., Koutsovitis, P., Zaccarini, F., Hauzenberger, C., Tsikos, H., Hatzipanagiotou, K. 2022. Post-magmatic processes recorded in bimodal chromitites of the East Chalkidiki meta-ultramafic bodies, Gomati and Nea Roda, northern Greece. Frontiers in Earth Science, 10:1031239.

Stella, A. 1924. Sopra un giacimento di cromite nel Vallone Argentiera presso Ziona (Alta Valle Vara). Bollettino della Societa Geologica Italiana 43,183–188.

Stevens, R. E. 1944. Composition of some chromites of the Western Hemisphere. American Mineralogist 29, l–34.

Stowe, C. W. 1994. Composition and tectonic settings of chromite deposits through time. Economic Geology 89, 528–546.

Tarkian, M., Economou-Eliopoulos, M., Eliopoulos, D. G. 1992. Platinum-group minerals and tetraauricupride in ophiolitic rocks of Skyros Island, Greece. Mineralogy and Petrology 47,55-66.

Thayer, T. P. 1970. Chromite segregations as petrogenetic indicators. In Symposium on the Bushveld Igneous Complex and Other Layered Intrusions; Geological Society of South Africa: Johannesburg, South Africa, 1970; 1, 380–390.

Zaccarini, F., Kiss, G. B., Garuti, G., Mauro, D., Economou-Eliopoulos, M., Hegedűs, M., Biagioni, C. 2025. Methane in fluid inclusions in ophiolitic chromitites revealed by Raman spectroscopy: preliminary results, 15, 335.

Zang, W., Fyfe, W. S. 1995. Chloritization of the hydrothermally altered bedrocks at the Igarape Bahia gold deposit, Carajas, Brazil. Mineralium Deposita 30, 30–38.

Zhou, M. F., Robinson, P. T. 1994. High-Cr and high-Al podiform chromitites from western China: Relationships to partial melting and melt/rock reaction in the upper mantle. International Geology Reviews 36, 678–686.

Zhou, M.-F., Sun, M., Keays, R. R., Kerrich, R. W. 1998. Controls on platinum-group elemental distributions of podiform chromitites: A case study of high-Cr and high-Al chromitites from Chinese orogenic belts. Geochimica Cosmochimica Acta 62, 677–688.